A Chromaticity Space for Specularity, Illumination Color- and Illumination Pose-Invariant 3-D Object Recognition

Daniel Berwick and Sang Wook Lee
(dberwick@umich.edu and swlee@umich.edu)
Dept. of Electrical Enginnering and Computer Science
University of Michigan
Ann Arbor, MI 48104

Abstract

Most of the recent color recognition/indexing approaches concentrate on establishing invariance to illumination color to improve the utility of color recognition. However, other effects caused by illumination pose and specularity on three-dimensional object surfaces have not received notable attention. We present a chromaticity recognition method that discounts the effects of illumination pose, illumination color and specularity. It utilizes a chromaticity space based on log-ratio of sensor responses for illumination pose and color invariance. A model-based *specularity detection/rejection algorithm can be used to improve the chromaticity recognition and illumination estimation for objects including specular reflections.*

1 Introduction

Reflectance-based recognition/indexing is a clear contrast to the previous recognition approaches. Traditional object recognition and viewing condition estimation uses geometric cues such as 3-D object shape models and geometric relationships between object features, and recent *appearance-based* approaches describe an object by using relatively compact eigenspaces derived only from image appearances under various viewing conditions [5] [17] [33] [25]. Although color reflectance has been conceived as an obvious object descriptor and color matching has been a central focus of color science and engineering, only recently have a number of researchers begun to explore the use of color distributions as signatures for object recognition. Their work has demonstrated that color can potentially be a strong cue [32] [26] [29] [14] [16] [30]. For image retrieval from an image database, color is one of the most effective cues [8] [1].

The early approaches for recognizing objects based on their color distributions were developed by Nagao *et al.* and by Swain and Ballard [26] [32]. Although this initial work does not address the problems of changing viewing conditions such as illumination direction and color change, it introduced the usefulness of color in recognition and motivated work for illumination color-invariant recognition. In order for object color to be stable to different illumination environments, variations in color distributions due to shading, lighting color, and specular reflections need to be discounted. The problem of color constancy for discounting illumination color to obtain reflectance color has been the topic of much research in psychology and computer vision [20] [34] [24] [13] [11]. The knowledge gained through color constancy research is reflected in recent recognition/indexing methods that explore illumination-invariant descriptors from color distributions.

Funt and Finlayson [14] developed *color-constant color indexing* (CCCI) to deal with scenes with variations in illumination color. By histogramming ratios of RGB values of adjacent pixels, they achieve a degree of color constancy that is relatively insensitive to illumination changes. Independently, Nayar and Bolle also used reflectance ratios for object recognition [29]. Healey *et al.* presented various methods mostly based on the affine property of color distribution change. By assuming a finite-dimensional linear surface reflectance model, changes in illumination color result in a linear transformation of global color pixel distributions in RGB space [16] [30] [31]. Their work has been extended to find local color features by restricting the spatial extent of regions in a color image.

In this paper, we present an approach for increasing the utility of color distributions and the impact of color-based recognition. Previous work paid little attention to color distribution changes due to illumination pose. A color histogram in RGB sensor space, or other linearly transformed three-dimensional space, when constructed as a 3-D binary occupancy grid is insensitive to viewing pose (barring occlusions). Geometric information is generally collapsed in a color histogram. However, changes in illumination direction can produce varying color distributions from a 3-D object. In previous work, most of the color features used are located on 2-D planar surfaces, or a fixed illumination pose is used for 3-D objects. Most color constancy work assumes a *Mondrian* world where shading change

depending on illumination pose is uniform throughout an image plane. It may be noted that the CCCI method is relatively insensitive to illumination change for smooth surface shapes, and that the problem of illumination pose-invariance is recently gaining attention [10] [23].

We suggest the use of intensity-normalized color space, i.e., chromaticity space, to discount changes in color distributions due to illumination pose. The space is based on the logarithms of sensor-response ratios, and chromaticity deformation due to illumination color change is limited to translation. We also address the problem of specularity in object color appearances. Previous research in color recognition assumes the lack of strong specularity and its effects in the color distribution. Detection of specularity has been a topic of active research in the field of physics-based vision [18] [15] [21] [3] [28] [2] [35] [27] [22]. Most of this work deals with basic modeling and algorithm development. We present a systematic method that couples specularity detection with color-based object recognition. In summary, we propose a color-based object recognition algorithm invariant to: (1) illumination pose, (2) illumination color, and (3) specularity. To our knowledge, the work that fully addresses these multiple problems simultaneously is scarce.

2 Illumination Pose-Invariance

As mentioned previously, a color histogram in the form of a multi-dimensional binary occupancy grid is invariant to mild change of viewing orientation and scale of the object within the image, assuming rotation does not result in a significantly different color distribution due to occlusion or disocclusion. This means that binary occupancy grid does not signify the number of pixels occupying the same color space. However, color distributions in the 3-D RGB occupancy grid may change their shape depending on object surface shading determined by illumination direction. If color features are distributed over surfaces with different orientations, a change in illumination direction results in nonuniform intensity changes among the color features. This illumination pose problem has been noted before, but has not been explicitly addressed.

A common representation of color distributions is a three-dimensional histogram as shown in Figure 1 (b). The axes measure responses to the RGB sensors of the camera in the range of visible light, $\lambda = 400nm$ to $700nm$, according to the equation

$$q_k = \int_\lambda (\boldsymbol{n}_s \cdot \boldsymbol{n}^{\boldsymbol{p}}) e(\lambda) s^{\boldsymbol{p}}(\lambda) Q_k(\lambda) d\lambda, \tag{1}$$

where $e(\lambda)$ is the illumination spectrum, $s^{\boldsymbol{p}}(\lambda)$ is the surface reflectance at the point $\boldsymbol{p}$, and Q_k and q_k for $k = 0, 1, 2$ or R, G, B are the spectral response and camera outputs, respectively. Surface shading is determined by the illumination direction vector $\boldsymbol{n}_s$ and the surface normal vector $\boldsymbol{n}^{\boldsymbol{p}}$. Only the diffuse reflection is included in the above model. The distribution of direct color sensor responses in a RGB space is affected by illumination pose. This is a consequence of surface normal variations on a 3-D object.

The relationship between sensor responses under different illumination colors can be modelled as a linear transform [16] [30]. For three-dimensional approximation of surface

reflection [6] [24],

$$s^{\boldsymbol{p}}(\lambda) = \sum_{i=0}^{2} \sigma_i^{\boldsymbol{p}} S_i(\lambda). \tag{2}$$

where S_i's are basis functions and σ_i's are weighting coefficients ($i = 0, 1, 2$), the sensor responses $\boldsymbol{q^p} = [q_R, q_G, q_B]^T$ and reflectance coefficients $\boldsymbol{\sigma^p} = [\sigma_0, \sigma_1, \sigma_2]^T$ are related as:

$$\boldsymbol{q^p} = [\boldsymbol{n}_s \cdot \boldsymbol{n^p}]\boldsymbol{\Lambda\sigma^p}, \quad \text{where} \quad \Lambda_{ki} = \int_\lambda e(\lambda) S_i(\lambda) Q_k(\lambda) d\lambda. \tag{3}$$

A change in illumination pose ($\widetilde{\boldsymbol{n}}_s$) and color ($\widetilde{\boldsymbol{\Lambda}}$) would result in a different set of sensor responses $\widetilde{\boldsymbol{q}}^{\boldsymbol{p}} = [\widetilde{\boldsymbol{n}}_s \cdot \boldsymbol{n^p}]\widetilde{\boldsymbol{\Lambda}}\boldsymbol{\sigma^p}$, and the transformation between the sensor responses is given as:

$$\widetilde{\boldsymbol{q}}^{\boldsymbol{p}} = r^{\boldsymbol{p}} \boldsymbol{M} \boldsymbol{q^p}, \tag{4}$$

where

$$r^{\boldsymbol{p}} = \frac{\widetilde{\boldsymbol{n}}_s \cdot \boldsymbol{n^p}}{\boldsymbol{n}_s \cdot \boldsymbol{n^p}}, \quad \text{and} \quad \boldsymbol{M} = \widetilde{\boldsymbol{\Lambda}}\boldsymbol{\Lambda}^{-1} \tag{5}$$

If the color measurements $\boldsymbol{q^p}$ are distributed over a 2-D planar surface, i.e., $\boldsymbol{n^p}$ is fixed for the surface points, the scaling factor due to shading is uniform. Therefore, the linear relationship, $\boldsymbol{M}$, between the sensor response vectors $\widetilde{\boldsymbol{q}}^{\boldsymbol{p}}$ and $\boldsymbol{q^p}$ holds. On the other hand, if the color measurements $\boldsymbol{q^p}$ are obtained from surface points with different orientations, the color values at these points will undergo different transformations because of different $\boldsymbol{n^p}$. Hence, the linear transform relationship is not appropriate for establishing illumination-color invariance for a general 3-D object.

A popular 2-D chromaticity space $\boldsymbol{x} = [x_1, x_2]^T$ is constructed by normalizing the sensor responses as:

$$x_1 = \frac{q_R}{q_R + q_G + q_B}, \quad x_2 = \frac{q_G}{q_R + q_G + q_B}, \tag{6}$$

In this projective space the scaling factor $r^{\boldsymbol{p}}$ due to shading disappears by the normalization, hence chromaticity is independent of illumination pose. This process removes the intensity component from the color distribution so that differences in shading are not distinguished.

Figure 1 shows a synthetic sphere under the same illumination color but with different illumination directions, and the RGB histograms and chromaticity diagrams of the sphere images. The RGB histograms may deform significantly when illumination pose varies for objects with different surface orientations. However, the chromaticity distribution remains the same.

3 Illumination Color-Invariant Chromaticity Space

The adoption of the chromaticity space initiates a new problem: identification of chromaticity signatures influenced by illumination color change. Differences in lighting color produce a nonlinear deformation of chromaticity descriptors due to the nonlinearity introduced by the normalization. Deformation of chromaticity signatures is governed by the transformation

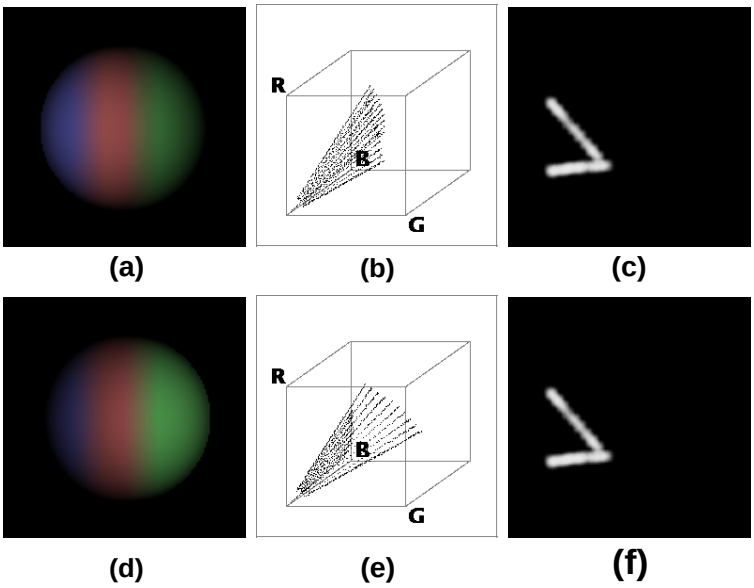

Figure 1: Effects of illumination pose (a,d) Illumination from the left and right, respectively, (b,e) RGB color histograms, (c,f) Chromaticity distributions

relationships in Equations 4 and 6. Formulation of invariance using the general matrix $\boldsymbol{M}$ in Equations 4 and the normalization in 6 may not be easily achieved. For establishing an illumination color-invariant chromaticity space, we simplify the chromaticity deformation based on the diagonal matrix transform which has long been proposed as a feasible mechanism for color constancy. Color constancy based on the diagonal matrix transformation and its impact are analyzed in detail by Finlayson, Drew and Funt, Worthey and Brill, West and Brill, and D'Zmura and Lennie [11] [12] [34] [7]. Finlayson, Drew and Funt showed that illumination change can be modelled as diagonal matrix transform under low-dimensional model constraints for illumination and reflectance [11].

Without the low-dimensional constraints on illumination and reflectance, the diagonal matrix transform can be approximated using very narrow color filters (ideally the Dirac delta function). If the filter function $Q_k(\lambda)$ in Equation 1 has a narrow bandwidth $\triangle Q_k$ around the wavelength λ_k and both $e(\lambda)$ and $s^{\boldsymbol{p}}(\lambda)$ are approximately constant within the filter bandwidth, the sensor responses can be approximated as

$$q_k \approx [\boldsymbol{n}_s \cdot \boldsymbol{n}^{\boldsymbol{p}}] e(\lambda_k) s^{\boldsymbol{p}}(\lambda_k) Q_m \triangle Q_k, \tag{7}$$

where Q_m is the magnitude of filter response. The relationship between the sensor responses $\boldsymbol{q^p}$ and $\tilde{\boldsymbol{q}}^{\boldsymbol{p}}$ (where $\tilde{q}_k = [\tilde{\boldsymbol{n}}_s \cdot \boldsymbol{n}^{\boldsymbol{p}}] e(\lambda_k) s^{\boldsymbol{p}}(\lambda_k) Q_m \triangle Q_k$) is given by a diagonal transform, i.e.,

$$\tilde{\boldsymbol{q}}^{\boldsymbol{p}} = r^{\boldsymbol{p}} \boldsymbol{D} \boldsymbol{q}^{\boldsymbol{p}}, \tag{8}$$

and the diagonal elements are given by

$$D_{00} = \tilde{e}(\lambda_0)/e(\lambda_0), \quad D_{11} = \tilde{e}(\lambda_1)/e(\lambda_1), \quad D_{22} = \tilde{e}(\lambda_2)/e(\lambda_2).$$

The diagonal matrix transform has been suggested as a base for many color constancy algorithms such as von Kries adaptation, retinex/lightness algorithms, and Forsyth's CRULE algorithm [34] [20] [13]. The narrow-band filters have been used successfully by Funt and Finlayson and by Nayar and Bolle [14] [29]. Finlayson, Drew, and Funt suggested methods for sharpening sensor functions and reported that the sensor sharpening improves the performance of color constancy algorithms based on diagonal transforms [12].

Under the diagonal transform condition, we suggest a chromaticity space $\boldsymbol{\xi} = [\xi_1, \xi_2]^T$ that is invariant to illumination color up to translation:

$$\xi_1 = ln\frac{q_R}{q_G}, \qquad \xi_2 = ln\frac{q_B}{q_G}, \tag{9}$$

In this space, the chromaticity distributions from an object under different illumination colors should appear identical up to translation, i.e.,

$$\tilde{\boldsymbol{\xi}} = \boldsymbol{\xi} + \boldsymbol{\eta}, \quad \text{where} \quad \boldsymbol{\eta} = [ln\frac{D_{00}}{D_{11}}, ln\frac{D_{22}}{D_{11}}]^T.$$

We use this space $\boldsymbol{\xi}$ for object identification and illumination estimation. The relationship between the chromaticity space $\boldsymbol{x}$ in Equation 6 and $\boldsymbol{\xi}$ is given as:

$$\xi_1 = ln\frac{x_1}{x_2}, \qquad \xi_2 = ln\frac{1 - x_1 - x_2}{x_2},$$

The use of reflectance ratios has been suggested previously in [14] and [29]. The CCCI approach utilizes the distribution of ratios from spatially neighboring pixels, and thus only the image regions where color values spatially vary contribute to the distribution effectively. Our log-sensor-ratio chromaticity space in Equation 9 uses the ratios of sensor responses from different bands at each surface point and the distribution of their logarithms as a signature for object identification. Therefore, all the color pixels are used to form the distribution regardless of their spatial variation. It may be noted that the descriptors used in homomorphic image processing of opponent colors are similar to the logarithm of sensor ratios, e.g., $ln(q_R/q_G)$ [9] [19]. Sensor ratios are also used for the gamut mapping method by Finlayson [10].

Although basic cross-correlation in $\boldsymbol{\xi}$ can be used for similarity measure, cross-correlation of test chromaticity distribution with all those of database objects would require high computational cost and estimation of $\boldsymbol{\eta}$ may be inaccurate if the correlation curve shows a broad peak. An alternative fast and accurate method is to use the Fourier magnitude spectrum for similarity measure and the Fourier phase for estimating $\boldsymbol{\eta}$ [4]. Let f be a chromaticity distribution function in the new coordinate system $\boldsymbol{\xi}$. The deformation by G results in the translation of f, i.e.,

$$f_G(\boldsymbol{\xi}) = f(\boldsymbol{\xi} + \boldsymbol{\eta}),$$

and their Fourier transforms will differ only in their phases:

$$\mathcal{F}[f_G(\boldsymbol{\xi})](\boldsymbol{\omega}) = e^{-i<\boldsymbol{\eta},\boldsymbol{\omega}>}\mathcal{F}[f(\boldsymbol{\xi})](\boldsymbol{\omega}) \tag{10}$$

Note that the magnitude of the Fourier spectrum $|\mathcal{F}[f_G(\boldsymbol{\xi})](\boldsymbol{\omega})|$ is invariant to $\boldsymbol{\eta}$. The phase term $Q(\boldsymbol{\omega})$ can be extracted by the following nonlinear filtering:

$$Q(\boldsymbol{\omega}) = e^{-i<\boldsymbol{\eta},\boldsymbol{\omega}>} = \frac{\mathcal{F}^*[f_G](\boldsymbol{\omega})\ \mathcal{F}[f](\boldsymbol{\omega})}{|\mathcal{F}[f_G](\boldsymbol{\omega})|\ |\mathcal{F}[f](\boldsymbol{\omega})|}, \tag{11}$$

and the inverse Fourier transform $q(\boldsymbol{\xi}) = \mathcal{F}^{-1}[Q(\boldsymbol{\omega})]$ will exhibit a peak at the illumination parameter $\boldsymbol{\eta}$ in the $\boldsymbol{\xi}$ domain.

4 Specularity Rejection

Specular reflections in an image may produce a substantial change in an object's chromaticity distribution. Strong specularities can significantly erode the similarity of chromaticity distributions between the model and test objects. Consequently, the illumination-invariance can be weakened. Although previous work in color-based recognition assumes lack of strong specularities, this problem needs to be addressed for reliable recognition.

The addition of specularity modifies sensor response in Equation 1 to be:

$$q_k = \int_\lambda e(\lambda)[(\boldsymbol{n}_s \cdot \boldsymbol{n}^{\boldsymbol{p}})s^{\boldsymbol{p}}(\lambda) + G_s^{\boldsymbol{p}} s_s^{\boldsymbol{p}}(\lambda)]Q_k(\lambda)d\lambda, \tag{12}$$

where $s^{\boldsymbol{p}}$ and $s_s^{\boldsymbol{p}}$ denote diffuse and specular reflection components, respectively. $G_s^{\boldsymbol{p}}$ represents the geometric factor for specular reflection, and is a function of many illumination, viewing and reflectance variables. In the chromaticity plane, specular reflections will appear as a cluster of points stretching from its underlying diffuse reflection chromaticity toward the chromaticity of the incident light (Figure 2 (a)) [2]. To avoid deviations from an object's chromaticity signature of only diffuse reflections, specularities need to be detected and removed from the test image. The goal of specularity detection is to find image regions where $s_s^{\boldsymbol{p}}$ is nonzero. "Specularity rejection" excludes the detected regions from the chromaticity signature.

Since specularity detection is not in general a well-constrained problem, most physics-based detection methods require restricting assumptions in object reflectance or need extra sensor data to provide physical constraints. These constraints include restricted material types and piecewise uniform object colors. Extra physical cues include structured light, polarization sensors, and multiple-view image sensing [18] [2] [21] [28] [35] [27] [22]. These additional requirements sensing may be difficult to achieve, especially for test images.

An additional source of information for specularity detection in lieu of extra sensing needs to be found. Our solution to this problem lies in the model images, from which we propose "model-based specularity detection/rejection". Using a potential match between the test object signature and a model object signature in the model base, a rough initial estimation of illumination color can be made. The chromaticity distribution of the test image can be compared with the model distribution considering the estimated illumination. From the comparison, some of the color clusters that ensue from specularity can be eliminated,

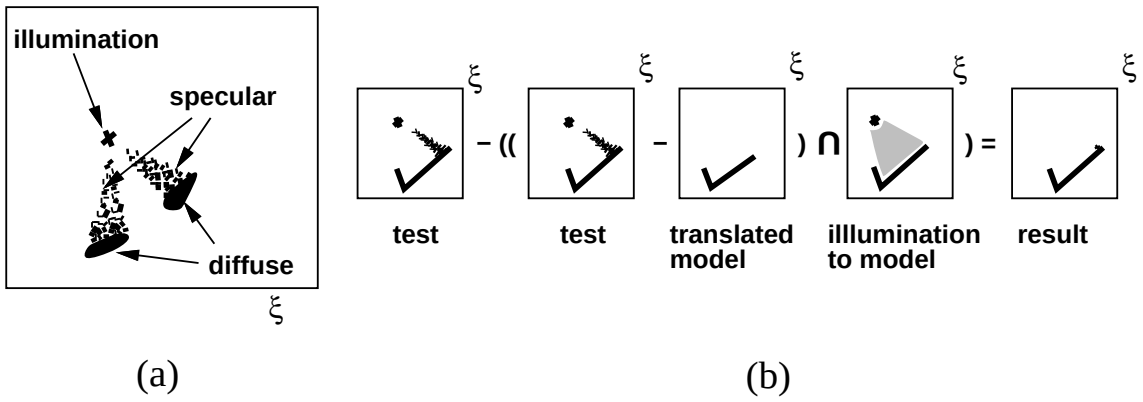

Figure 2: (a) Effect of specularities in chromaticity plane. (b) Chromaticity differencing from illumination estimation

and the illumination estimation can be refined and used to emend further the chromaticity distribution. This chromaticity histogram comparison is motivated by *histogram differencing* techniques [21] [22].

Our approach to specularity rejection begins with conservative intensity-based processing of a test image, such as intensity thresholding, to eliminate sharp and intense specularity without any prior information [3]. From the resulting signature, a hypothesis for initial object identification and illumination estimation is generated. This signature is iteratively refined by *chromaticity differencing*.

Figure 2 (b) illustrates this differencing process. Based on the identified object and initial illumination estimation after thresholding, the chromaticity plane associated with the object and estimated illumination is used for coarse differencing with the test chromaticity diagram.

The difference between two signatures can be computed by subtracting the potential model signature from the test signature. The result of this operation are the chromaticities that may be the result of specularity. Of these chromaticities, those that lie between a part of the model signature and the estimated illumination are considered to be caused by specularity. A new signature for the test object is created that removes parts of the signature considered to be specularity.

Since differencing produces a chromaticity plane that is less affected by specularities, the peak value of $|q(\boldsymbol{\xi})|$ may increase and may yield a more accurate illumination estimate. This result drives the process into another round of differencing. By iteratively refining the chromaticity diagram of the test object by specularity removal, the peak value of $|q(\boldsymbol{\xi})|$ keeps increasing if the hypothesized object is indeed correct. For an incorrect hypothesis, the refinement process will terminate with the decreased peak value of $|q(\boldsymbol{\xi})|$. The specularity rejection algorithm is initiated when there is no dominant match to the objects in the database. The test is differenced with each of the best matching objects. The specularity

rejection algorithm is summarized as follows.

1. Apply a conservative intensity threshold T_I for initial specularity rejection, and compute $q(\boldsymbol{\xi})$.

2. If the peak $|q(\boldsymbol{\xi})|_{max}$ is within some percent threshold T_S, of the highest $|q(\boldsymbol{\xi})|_{max}$ of the database, estimate an initial illumination color $\boldsymbol{\eta}$.

3. Using $\boldsymbol{\eta}$, translate the model chromaticity signature and do chromaticity differencing using the illumination estimation and the model signature to determine the region of specularity.

4. Create the new test signature

5. Compute $|q(\boldsymbol{\xi})|_{max}$ of the new test signature and update $\boldsymbol{\eta}$.

6. While the peak $|q(\boldsymbol{\xi})|_{max}$ increases, repeat steps 3, 4, 5, and 6. Otherwise, stop.

The thresholds T_I and T_S are fixed and predetermined.

When the object match is correct and the illumination estimations are reasonable, iterative specularity removal will keep the peak $|q(\boldsymbol{\xi})|_{max}$ increasing. If the deformation by the presence of specularity is too severe and initial intensity thresholding does not make a difference, this process simply stops immediately, and a test object remains unidentified.

5 Experimental Results

The proposed $\boldsymbol{\xi}$ chromaticity space and specularity rejection algorithm are tested using a database of eight objects. The objects are illuminated with two 500 Watt, 3200 K, GE Photofloods mounted in reflected scoops. Digital Images are gathered with a Sony XC-77RR and color images are generated from this greyscale camera using a set of relatively narrow-band RGB filters. These are Kodak Wratten filters numbers 29, 47, and 61. The aperture of the camera is adjusted for each object to prevent saturation, and .3 neutral density gel is added to the red and green filters to more closely match the transmission of the blue filter. The illumination color is altered by placing gel filters in front of the lamps. There is some variation in the illumination of object scenes. The filters cannot not be placed close enough to lamps to prevent all the unfiltered light from falling on the object. Although we are unable to measure the effects of this ambient illumination, the chromaticity descriptions are still unique enough for recognition.

The database images are taken with the illumination filtered by Lee Filter 201 (Full CT Blue) which moves the incandescent light towards a neutral color. Specularities in the model images are removed by intensity thresholding methods [21] or by hand before the chromaticity descriptors are created. Figure 3 (a), (b) and (c) show the database objects, their chromaticity diagrams in the $\boldsymbol{x}$ space, and in the $\boldsymbol{\xi}$ space, respectively. The range of the $\boldsymbol{\xi}$ chromaticity space is from -∞ to ∞ along the ξ_1 and ξ_2 axes. A square window is

	cyl	gel	gun	gun'	horse	nut	pad	pea	tooth
cyl	**.34**	**.32**	.31	.33	**.33**	.26	.27	.29	**.31**
gel	.29	**.33**	.29	.35	.32	.28	**.31**	.34	.27
gun	.29	.29	**.38**	**.39**	**.34**	.31	.29	.30	.27
horse	.30	**.34**	**.38**	**.39**	**.36**	**.35**	**.32**	.32	**.33**
nut	.27	.29	.27	.29	.28	.26	.28	.28	.25
pad	.28	.30	.29	.32	.29	.27	.30	.30	**.33**
pea	.25	.27	.30	.31	.28	.26	.26	**.37**	.24
tooth	.23	.27	.29	.28	.27	.25	.29	.29	.27

Table 1: Results from the $\boldsymbol{x}$-chromaticity diagrams

	cyl	gel	gun	gun'	horse	nut	pad	pea	tooth
cyl	**.82**	.57	.43	.46	.58	.53	.50	.56	.47
gel	.64	**.87**	.52	.55	.70	.70	.69	.66	.64
gun	.50	.52	**.83**	**.82**	.59	.45	.61	.58	.44
horse	.66	.77	.61	.66	**.90**	.71	.78	.71	.59
nut	.57	.73	.51	.55	.73	**.90**	.69	.73	.66
pad	.51	.67	.60	.69	.77	.56	**.84**	.56	.59
pea	.72	.72	.54	.61	.76	.76	.70	**.88**	.63
tooth	.54	.64	.51	.52	.69	.72	.66	.68	**.84**

Table 2: Results from the $\boldsymbol{\xi}$-chromaticity diagrams

placed over the $\boldsymbol{\xi}$ chromaticity space ranging from -4.0 to 4.0. Test images are created by varying the pose of the new objects and by not filtering the incandescent light. Test images, their chromaticity diagrams in the $\boldsymbol{x}$ space and in the $\boldsymbol{\xi}$ space are shown in Figure 3 (d), (e) and (f), respectively. Some of the test images contain specularities while some do not. These test objects are then used to test the illumination pose and color invariance. Notice that the $\boldsymbol{x}$-chromaticity diagrams show substantial deformation between the database and test objects while the $\boldsymbol{\xi}$-chromaticity diagrams do not.

To provide a reference for the $\boldsymbol{\xi}$-chromaticity performace, the $\boldsymbol{x}$-chromaticity performance is tested, and the results are shown in Table 1. The leftmost column represents the database objects under the reference light and the top row the test objects under the unfiltered incandescent light. For the plastic gun, an extra pose is generated for more specularities (denoted by "gun' "). The data entries in the table are correlation values between the test and database objects. Not surprisingly, this approach does not perform very well. Because the test images are taken under a different illumination color, the $\boldsymbol{x}$ diagrams are deformed beyond a simple translation. Of the nine test images only three are recognized successfully. Six of the tests images are marked as non-distinct because the test image returns matched values within ten percent of each other. The results provide a reference to judge the effect of the $\boldsymbol{\xi}$ chromaticity space.

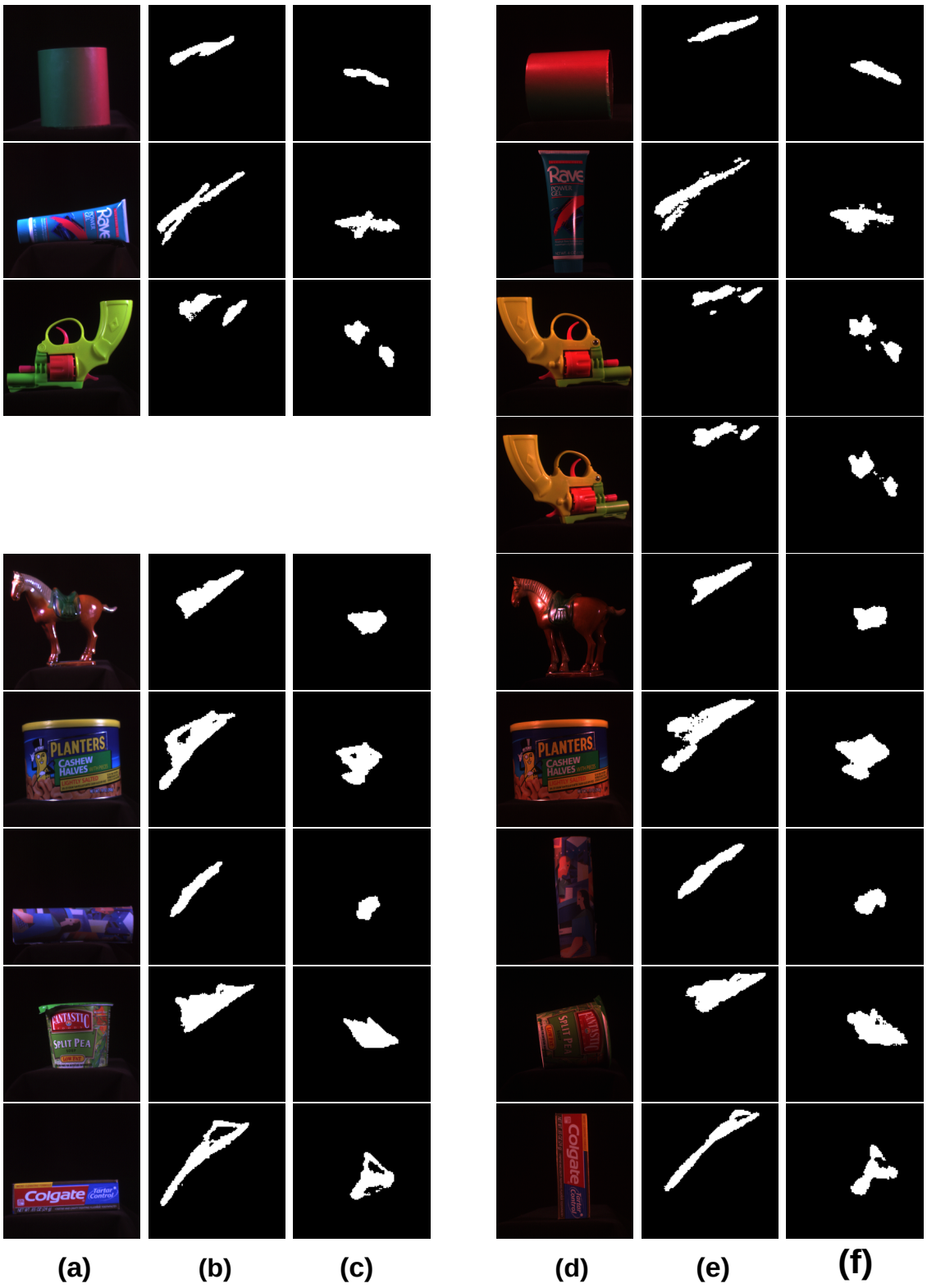

Figure 3: (a) Database objects, (b) $\boldsymbol{x}$ chromaticity diagrams, (c) $\boldsymbol{\xi}$ chromaticity diagrams, (d) test objects, (e) $\boldsymbol{x}$ chromaticity diagrams, and (f) $\boldsymbol{\xi}$ chromaticity diagrams. Color versions of columns (a) and (d) are available at http://vision.ai.eecs.umich.edu/vision/database.html

	$\boldsymbol{x}$-chromaticity	$\boldsymbol{\xi}$-chromaticity
No. of Tests	9	9
No. Recog	3	9
No. Non-distinct	6	0
Average Rank	1.2	1

Table 3: Summary of results from $\boldsymbol{x}$-chromaticity and $\boldsymbol{\xi}$-chromaticity diagrams

The matching results from the $\boldsymbol{\xi}$ chromaticity diagrams are shown in Table 2. The algorithm showed significant improvement over the $\boldsymbol{x}$ chromaticity method. All except one of the test images are correctly matched. The remaining image, of the gel (which contained significant specularities), is originally marked non-distinct because two high match values are returned. Even though the algorithm cannot determine with certainty which object is in the test image, it is aware of its failure. Our specularity detection/rejection method was applied to the non-distinct test image and the two best matching model images: the gel and the horse. The differencing increased the correlation of the test image with the gel model, but did not change the correlation with the model horse image. Table 3 summarizes the performance of the $\boldsymbol{x}$ and $\boldsymbol{\xi}$ chromaticity spaces in terms of some measures:"No. Recog", and "No. Non-distinct" denote the number of times the algorithm correctly recognizes a test object and cannot distinguish between matches, respectively, and the rank is the position of the correct matching in the sorted list of match values.

6 Discussion

Chromaticity representations of object colors discount object shading variation that results from illumination pose change. It is our intent to separate the color information from geometric information that is otherwise confounded in RGB values. The proposed log-sensor-ratio chromaticity space further provides illumination color invariance up to translation and our specularity rejection method reduce the influence of specular reflections on chromaticity distribution.

Methods that are based on reflectance ratios and narrow-band filters have been suggested previously by Funt and Finlayson [14] and Nayar and Bolle [29]. The main difference is that the proposed log-sensor-ratio method creates the signature from the ratio of different color bands at the same pixel, while the previous ratio-based methods use ratios of different pixels in the same color band. Another difference is that the previous ratio-based methods concentrate only on image regions where color varies substantially, such as color edges, and do not utilize uniformly colored areas. If surface orientations do not vary over neighboring pixels, the previous reflectance-ratio methods achieve illumination color and pose invariance. This invariance occurs because the illumination and surface normal are considered to be the same for the pixels used in the ratio and hence only the ratio of object color remains. However, if the surface normals are not the same, then the ratio will not be invariant. The

different shading that may result from altering the incident light configuration will cause the ratios to vary. This may occur where surface orientation changes substantially such as vertices of polyhedral objects. Our proposed method eliminates this problem by eliminating the effects of shading using the chromaticity space. On the other hand, the previous ratio-based methods require only local illumination color uniformity and less sensitive to gradual change of illumination color across a scene. Varying illumination in the log-sensor-ratio chromaticity space will cause different pixels to experience a different translation $\boldsymbol{\eta}$. These differing translation will cause the signature to warp beyond a simple translation of the model signature. Thus, the log-sensor-ratio space can only be effective if illumination color is uniform throughout the scene.

In this paper, we introduce a specularity rejection method that is closely coupled with illumination color-invariant chromaticity matching. To our knowledge, specularity has not been addressed by previous methods. We assume that specularity is localized in space (specular spike) and does not fully occlude critical colors in diffuse reflections. The color distribution is in general insensitive to partial occlusions since a color distribution signature is generated from a whole object surface. Slight color variation due to spatially extended but weak luster is regarded as noise. Beyond this condition, our method adds chromaticity differencing to help reduce the effect of specularity. In a test image containing specularity, the specular region will add chromaticity clusters ranging from the object chromaticity to the illumination chromaticity. These additional chromaticities should appear as an additional lobe to the model signature. Chromaticity differencing forces the test signature to be closer to the model signature eliminating lobes that extend from model chromaticity clusters to illumination chromaticity.

7 Conclusion

To effectively employ color information as a reliable descriptor of an object for recognition, color reflectance intrinsic to the object surface should be extracted, and the variation of color appearance due to viewing and illumination pose, illumination color, and specularity needs to be discounted. We propose the use of a chromaticity space based on log-sensor-ratio of sensor responses for illumination-pose and illumination-color invariance. We also suggest a specularity rejection method based on chromaticity differencing. Experimental results are presented to demonstrate the efficacy of the proposed chromaticity space and specularity rejection method.

References

[1] J.R. Bach, C. Fuller, A. Gupta, A. Hampapur, R. Horowitz, R. Humphrey, R.C. Jain, and C. Shu. Virage image search engine: An open framework for image management. In *Proc. SPIE Storage and Retrieval of Still Image and Video Databases IV*, pages 76–87, San Jose, CA, 1996.

[2] R. Bajcsy, S.W. Lee, and A. Leonardis. Detection of diffuse and specular interface reflections and inter-reflections by color image segmentation. *IJCV*, 17, 1996.

[3] G. Brelstaff and A. Blake. Detecting specular reflections using lambertain constraints. In *Proc. of IEEE Int. Conf. on Computer Vision*, pages 297–302, Tarpon Springs, FL, 1988.

[4] Q.S. Chen, M. Defrise, and F. Deconinck. Symmetric phase-only matched filtering of fourier-mellin transforms for image registration and recognition. *IEEE Trans. PAMI*, 16:1156–1168, 1994.

[5] R.T. Chin and C.R. Dyer. Model-based recognition in robot vision. *ACM Computing Surveys*, 18, 1986.

[6] J. Cohen. Dependency of the spectral reflectance curves of the munsell color chips. *Psychon. Sci.*, 1:369–370, 1964.

[7] M. D'Zmura and P. Lennie. Mechanisms of color constancy. *JOSA*, 3:1662–1672, 1986.

[8] M. Flickner et al. Query by image and video content: The qbic system. *IEEE Computer*, 28:23–32, 1995.

[9] O.D. Faugeras. Digital color image processing within the framework of a human visual model. *IEEE Trans. ASSP*, 27:380–393, 1979.

[10] G. D. Finlayson. Color in perspective. *IEEE Trans. PAMI*, 18(10):1034–1038, 1996.

[11] G. D. Finlayson, M. S. Drew, and B. V. Funt. Color constancy: Generalized diagonal transforms suffice. *JOSA*, 11:3011–3019, 1994.

[12] G. D. Finlayson, M. S. Drew, and B. V. Funt. Spectral sharpening: Sensor transformations for improved color constancy. *JOSA*, 11:1553–1563, 1994.

[13] D. A. Forsyth. A novel approach to colour constancy. *IJCV*, 5:5–36, 1990.

[14] B. V. Funt and G. D. Finlayson. Color constant color indexing. *IEEE Trans. PAMI*, 17:522–529, 1995.

[15] G.H. Healey. Using color for geometry-insensitive segmentation. *JOSA*, 6, 1989.

[16] G.H. Healey and D. Slater. Global color constancy: Recognition of objects by use of illumination-invariant properties of color distributions. *JOSA*, 11, 1994.

[17] D.P. Huttenlocher and S. Ullman. Recognizing solid objects by alignment. *IJCV*, 5, 1990.

[18] G.J. Klinker, S.A. Shafer, and T. Kanade. A physical approach to color image understanding. *IJCV*, 4, 1990.

[19] J.J. Koenderik, W.A. van de Grind, and M.A. Bouman. Opponent color coding: A mechanical model and a new metric for color space. *Kybernetik*, 10:78–98, 1972.

[20] E.H. Land and J. J. McCann. Lightness and retinex theory. *JOSA*, 61:1–11, 1971.

[21] S.W. Lee and R. Bajcsy. Detection of specularity using color and multiple views. *Image and Vision Computing*, 10:643–653, 1992.

[22] S. Lin and S.W. Lee. Detection of specularity using stereo in color and polarization space. *Computer Vision and Image Understanding*, 1997.

[23] S. Lin and S.W. Lee. Using chromaticity distributions and eigenspace for pose-, illumination-, and specularity-invariant 3d object recognition. In *To Appear in Proc. IEEE Conf. Compt. Vision and Pattern Recog.*, 1997.

[24] L. T. Maloney and B. A. Wandell. A computational model of color constancy. *JOSA*, 1:29–33, 1986.

[25] H. Murase and S.K. Nayar. Visual learning and recognition of 3-d objects from appearance. *IJCV*, 14, 1995.

[26] M. Nagao, T. Matsuyama, and Y. Ikeda. Region extraction and shape analysis in aerial images. *CGIP*, 10(3):195–223, July 1979.

[27] S. K. Nayar, X. S. Fang, and T. Boult. Separation of reflection components using color and polarization. In *Proc. DARPA IU Workshop*, pages 1049–1060, Washington, DC, 1993.

[28] S. K. Nayar, K. Ikeuchi, and T. Kanade. Determining shape and reflectance of hybrid surfaces by photometric sampling. *IEEE Trans. Robo. Autom.*, 6:418–431, 1990.

[29] S.K. Nayar and R.M. Bolle. Reflectance based object recognition. *IJCV*, 17, 1996.

[30] D. Slater and G.H. Healey. The illumination-invariant recognition of 3d objects using local color invariants. *IEEE Trans. PAMI*, 18(2), 1996.

[31] D. Slater and G.H. Healey. Using spectral reflectance model for the illumination-invariant recognition of local image structure. In *Proc. CVPR*, pages 770–775, 1996.

[32] M. J. Swain. Color indexing. *IJCV*, 7:11–32, 1991.

[33] M.A. Turk and A. Pentland. Face recognition using eigenfaces. In *Proc. CVPR*, pages 586–591, 1991.

[34] G. West and M.H. Brill. Necessary and sufficient conditions for von kries chromatic adptation to give colour constancy. *J. Math. Biol.*, 15:249–258, 1982.

[35] L. B. Wolff. Using polarization to separate reflection components. In *Proc. of CVPR*, pages 363–369, San Diego, 1989.